Insights in brine dynamics and sea-ice desalination from a 1D model study of gravity drainage

Philipp J. Griewank , Dirk Notz

2013

Abstract

We study gravity drainage using a new one-dimensional, multi-phase sea-ice model. A parametrization of gravity drainage based on the convective nature of gravity drainage is implemented and is able to reproduce laboratory salinity measurements. We find a strong link between sea-ice growth rate and bulk salinity for constant boundary conditions, but only a weak link for more realistic boundary conditions. We also demonstrate that surface warming can trigger brine convection over the whole ice layer. To quantify the relevance of gravity drainage to climate models, we simulate a growth season with and without the convective parametrization. In these simulations, replacing the convective parametrization with constant initial salinities leads to an overall 7 % overestimation of stored energy, thermal resistivity, and salt release over a growth season. To reduce this overestimation of 7 %, we introduce an additional gravity-drainage parametrization as a numerically cheap and stable alternative for climate sea-ice models. This additional parametrization is a simplification of the convective parametrization and results in a 4 % overestimation of stored energy, thermal resistivity, and salt release compared to the convective parametrization.

1 Introduction

Gravity drainage, which is the convective exchange of cold and dense brine with fresher seawater, is the dominant desalination process in sea ice [*Notz and Worster*(2006), *Notz and Worster*(2009),] and plays a crucial role in sea-ice biogeochemistry by replenishing the ice with nutrients [*Vancoppenolle et al.*(2010) *Vancoppenolle, Goosse, de Montety, Fichefet, Tremblay, and Tison*,]. It has also been proposed to utilize gravity drainage to desalinate sea water efficiently [*Gu et al.*(2012) *Gu, Lin, Xu, Yuan, Tao, Li, and Liu*,]. In this paper, we study gravity drainage using the newly developed 1D thermodynamic sea-ice model SAMSIM (Semi-Adaptive Multi-phase Sea-Ice Model)

with a convective gravity drainage parametrization. The model is used in particular to quantify how gravity drainage affects the thermodynamic properties of sea ice. We also present a simplified salinity parametrization based on our convective parametrization that is suitable for climate models.

Our current understanding of gravity drainage is far from complete, partly because detailed measurements of brine flow in sea ice are largely lacking. Most of our current understanding stems from evaluating salinity measurements from ice cores and laboratory studies of growing multi-phase materials [*Chen*(1995), *Wettlaufer et al.*(1997) *Wettlaufer, Worster, and Huppert*, *Cottier et al.*(1999) *Cottier, Eicken, and Wadhams*, e.g.]. However, growing and measuring sea ice in the laboratory over many weeks is a practical challenge, and (to our knowledge) no laboratory sea-ice experiments lasting longer than a month have been conducted.

Detailed field studies of growing sea ice through ice core series are rare owing to the severe logistical issues of taking and processing ice cores under extremely inhospitable climate conditions. Hence, only few such studies exist, most notably are those conducted by [*Nakawo and Sinha*(1981),], [*Lei et al.*(2010) *Lei, Li, Cheng, Zhang, and Heil*,] and [*Gough et al.*(2012) *Gough, Mahoney, Langhorne, Williams, and Haskell*,]. Unfortunately, measuring salinity by ice cores has many drawbacks. These include brine loss from cores, low temporal resolution, and the inability to sample repeatedly due to the destructive nature of core extraction. [*Gough et al.*(2012) *Gough, Mahoney, Langhorne, Williams, and Haskell*,] conducted a very thorough analysis of their core data showcasing that, due to the high horizontal variability and vertical dependency in salinity anomaly measurements, multiple cores are necessary to obtain representative values.

In this paper we study gravity drainage numerically. Previous numerical studies can be split into 2D approaches, which simulate the flow field of brine in a vertical slice of growing sea ice, and 1D approaches, which parametrize the brine flow and its effects on the vertical sea-ice profile. 2D models have the drawback of being computationally expensive and/or limited to well defined test cases [**?**, see]]Oertling2004,Petrich2004,Wells2010. Proposed 1D parametrizations are either based on the quantitative estimates of [*Cox and Weeks*(1988),], or treat gravity drainage as a turbulent diffusion process [*Vancoppenolle et al.*(2010) *Vancoppenolle, Goosse, de Montety, Fichefet, Tremblay, and Tison*, *Jeffery et al.*(2011) *Jeffery, Hunke, and Elliott*,]. However, both of these 1D methods are inconsistent with laboratory experiments and 2D simulations from which we know that gravity drainage is not a turbulent process. [*Saenz and Arrigo*(2012),] were the first to take the convective nature of gravity drainage partially into account, but their gravity drainage parametrization is still based on the simplified estimates of [*Cox and Weeks*(1988),].

Our approach extends the findings of small-scale laboratory experiments and 2D numerical simulations to larger and longer scales using a 1D thermodynamic model based on mushy-layer theory and a convective gravity drainage parametrization derived from research on brine fluxes from solidifying binary alloys [*Wells et al.*(2010) *Wells, Wettlaufer, and Orszag*,]. A key property of the

newly developed thermodynamic multi-phase model SAMSIM is a semi-adaptive grid, which gives us an advantage over previous attempts to parametrize gravity drainage. Instead of prescribing an explicit ice-ocean front, as in the Maykut and Untersteiner model [*Maykut and Untersteiner*(1971),] and all its descendants [**?**, e.g.]]Semtner1976,Bitz1999,Huwald2005a, the grid ensures that the ice-ocean interface is always well resolved without imposing any assumptions of salinity, temperature or growth rate. Open questions we address in this paper are the link between sea-ice growth speed and bulk salinity, if gravity drainage can penetrate deep into the ice, and how gravity drainage can be represented in climate models.

The convective parametrization is ill-suited for earth system models as it requires a small time step to avoid instabilities. As an alternative we derive a simpler parametrization from the convective as a tool to improve sea-ice thermodynamics and salt release into the ocean for climate models. In this paper we refer to the simpler salinity parametrization as the simple parametrization and to the more complex parametrization that calculates brine fluxes as the convective parametrization.

Section 2 provides a brief description of SAMSIM. In section 3 we intorduce the full convective parametrization. Based on it, we also devise a simple salinity parametrization of gravity drainage which is a computationally cheap alternative for climate models. Section 4 contains a description of the Levenberg-Marquadt optimization process algorithm and data used to determine the free parameters of our parametrizations. In section 5 we conduct our first experiments using idealized boundary conditions. Here we study how growth speeds influence bulk salinity and how deep convection can be triggered. These findings are then compared to a more realistic growth season simulated by forcing the model with three-hourly ERA-reanalysis data in section 6. Using this growth season, we study how the thermal properties of the sea ice vary when the salinity is either prescribed, or simulated using the simple parametrization that we introduced in section 3. Finally, in section 7, we present a summary of our results and conclusions, and discuss how gravity drainage can be represented in climate models.

2 SAMSIM description

In the following section we provide a brief overview of SAMSIM, our semi-adaptive multi-phase sea-ice model. The thermodynamic core of SAMSIM is derived from the mushy-layer equations of sea ice [*Feltham et al.*(2006)*Feltham, Untersteiner, Wettlaufer, and Worster*,]. Our approach is similar to that of [*Notz and Worster*(2006),], but was extended to also include a gas phase and gravity drainage. For an in depth discussion on multi-phase sea-ice models see [*Hunke et al.*(2011)*Hunke, Notz, Turner, and Vancoppenolle*,].

In contrast to commonly used front tracking models [**?**, see]]Maykut1971,Semtner1976,Bitz1999,Huwald2005a SAMSIM has no prescribed ice-ocean front. Instead, SAMSIM uses the alternative approach of resolving the ice-ocean interface. Although there are many

reasons to prefer the front-tracking approach, resolving the ice-ocean interface grants us a bit of additional freedom which we exploit when parametrizing brine dynamics. Additionally, we believe there is a simple theoretical elegance in simulating solid fractions without explicitly treating sea-ice and ocean water as separate materials.

SAMSIM is a finite-volume model to allow simple conservation of all conserved properties, such as mass, energy, and tracers. Currently, the spatial and temporal discretisation schemes to solve the heat transport equation

$$q = -k\frac{\partial T}{\partial z}$$

are of first-order and require a small time step. Higher order schemes can be implemented if a longer time step is needed.

2.1 Layer properties

SAMSIM is a 1D finite-volume model, in which each layer is in thermal equilibrium and horizontally and vertically homogeneous. Each layer is defined by four core variables: absolute salinity S_{abs}, absolute enthalpy H_{abs}, mass m, and thickness $\triangle z$. From the absolute salinity, absolute enthalpy and mass we derive temperature T and solid mass fraction ψ by numerically solving the following set of equations for enthalpy (H), bulk salinity (S_{bu}), brine salinity (S_{br}), and ψ:

$$H = \frac{H_{abs}}{m} = -\psi L + f(T) \tag{1}$$

$$S_{bu} = \frac{S_{abs}}{m} = S_{br}(1-\psi) \tag{2}$$

$$S_{br} = g(T) \tag{3}$$

The appropriate value of latent heat (L) and the empirical functions of temperature ($f(T), g(T)$) are material dependent and their accuracy can be varied as desired. By approximating gas as massless, we can derive the solid, liquid, and gas phase volume fractions (ϕ_s, ϕ_l, and ϕ_g) from ψ, $\triangle z$, and m.

Salt is treated as a massless tracer but brine density is a function of brine salinity. When brine moves between layers, salt advection is calculated via the simple upstream method. The simple upstream method is artificially diffusive, especially when the tracer concentration has steep gradients. Since the brine salinity is determined by the temperature and the temperature profile in sea ice is rather smooth, the artificial diffusion for salinity is small. If passive tracers were introduced, a more sophisticated advection method might be needed.

The thermal conductivity of each layer is simply the volume weighted sum of the solid and gas fractions $k = \phi_s k_s + \phi_l k_l$. The gas fraction is treated as a perfect isolator and doesn't contribute to the layer's conductivity.

2.2 Semi-adaptive grid

SAMSIM employs an irregular 1D grid which we refer to as a semi-adaptive grid for lack of a better term. This grid consists of a set number of top and bottom layers (N_{top} and N_{bot}) with a constant thickness of $\triangle z_0$, and a number of adaptive middle layers (N_{mid}) which grow and shrink in steps of $\triangle z_0/N_{mid}$ as needed. When the ice is so thin that not all layers are needed surplus layers are deactivated. As long as the number of active layers (n) is less or equal to the maximum number of layers (N=$N_{top} + N_{mid} + N_{bot}$), all active layers share the thickness $\triangle z_0$. If no ice is present at all, SAMSIM shrinks to a single layer. The layers are indexed from top to bottom. This means that the index i of the top layer is 1, the lowest active layer has the index n, and when all layers are active the lowest layer has the index N.

Figure 1 shows how SAMSIM's semi-adaptive grid evolves during growth for N=5, N_{top}=1, N_{mid}=2, N_{bot}=2. Starting from a single layer of open water (n=1), the grid grows to ensure that the solid volume fraction ϕ_s^n in the lowest active layer always lies below a certain fixed value ($\phi_s^n < \phi_s^{min}$). When ϕ_s^n increases beyond the limit value ϕ_s^{min} a new layer of underlying ocean water is added. If not all layers are activated ($n < N$) the new layer is created by activating one of the previously deactivated layers. If $n = N$ then the uppermost bottom layer is merged into the middle layers changing $\triangle z$ accordingly, and all the bottom layers are shifted downwards by one. Conversely, the lowest layer is dissolved when ϕ_s^n=0 and $\phi_s^{n-1} < \phi_s^{min}/2$. The lowest layer is dissolved only when $\phi_s^{n-1} < \phi_s^{min}/2$ to ensure that new layers are not dissolved shortly after forming, when ϕ_s^n=0 and $\phi_s^{n-1} \approx \phi_s^{min}$. It is possible to set ϕ_s^{min} to zero, but under certain conditions this can lead to many bottom layers with very low solid fractions. In nature these very low solid fractions would indicate free floating ice crystals. ϕ_s^{min} can be understood physically as the minimum amount of ice needed for the ice crystals to form a connected mushy layer.

The semi-adaptive grid has three major advantages. First, it allows SAMSIM to keep the spatial resolution constantly high at the ice-ocean and ice-atmosphere boundaries without exceeding a set maximum amount of layers. The second advantage is that no numerical diffusion occurs in the bottom layers due to moving layer boundaries. Instead, newly formed bottom layers retain their salinity, enthalpy and mass as they are shifted upwards in steps until they are merged into the middle layers. The final advantage is that the lowest layer — which represents the water at the ice-ocean interface— can evolve freely, which lets SAMSIM imitate processes such as underplating to a certain extent.

For the aims of this study, these advantages of the semi-adaptive grid far outweigh its disadvantages. These disadvantages include temporal discontinuities in the simulations caused by the finite-size, step-wise addition and removal of layers. Additionally, vertical tracer advection across the transition from thin to thicker layers can cause nonphysical tracer transport. However, these numerical artifacts are small and can safely be neglected in this paper, since gravity drainage is mostly localized to the thin bottom layers. A further disadvantage of SAMSIM's grid are possible difficulties in its horizontal advection, which, again,

is irrelevant for our one-dimensional study. Finally, SAMSIM's grid causes a somewhat larger computational burden compared to traditional grids, because the thin top and bottom layers limit the time step.

For specific purposes, such as calculating the ice thickness, we require a defined ice-ocean front which is not provided a-priori by SAMSIM's grid. For such purposes we linearly interpolate a value from the solid volume fraction of the lowest layer. For example, if $\phi_s^n = \phi_s^{min}/3$, we would assume the upper third of the bottom layer to contain sea ice.

For the purpose of this paper, snow is treated as a single layer of varying thickness with constant density and constant thermal conductivity. Although this simple setup is still standard for sea-ice components of earth system models, there have been recent pushes to include more sophisticated representations of snow in climate models [*Lecomte et al.*(2011)*Lecomte, Fichefet, Vancoppenolle, and Nicolaus*,].

2.3 Brine expulsion

Because the density of ice is lower than that of water, freezing sea ice expels excess brine. This process is known as brine expulsion and was once believed to be an important desalination process in thin ice [*Cox and Weeks*(1975),]. [*Notz and Worster*(2006), *Notz and Worster*(2009),] have demonstrated that although brine expulsion redistributes salt in the sea ice, the amount of salt that leaves the ice is negligibly small. However, brine expulsion is crucial to the density evolution of sea ice.

SAMSIM determines the amount of brine which is expelled by checking if the summed volume of liquid brine and solid ice exceeds the volume of the layer at each time step. If the volume does exceed the layer volume SAMSIM assumes that the excess brine is always moved to the layer below, regardless of the properties of the lower layers. In reality, brine can move upwards as well. Upward displaced brine can cause thin skins of extremely salty brine on top of the sea ice, a behavior [*Roscoe et al.*(2011)*Roscoe, Brooks, Jackson, Smith, Walker, Obbard, and Wolff*,] captured with time-lapse photography. However, since the total amount of salt transported by upward displaced brine is comparably small, we expect the salinity errors in SAMSIM introduced by our unidirectional implementation of brine expulsion to be small.

3 Gravity drainage parametrizations

In contrast to 2D or 3D models, a 1D model is incapable of resolving a convective process and gravity drainage can only be parametrized. Previous one-dimensional parametrizations of gravity drainage were presented by [*Cox and Weeks*(1988),],[*Vancoppenolle et al.*(2010)*Vancoppenolle, Goosse, de Montety, Fichefet, Tremblay, and Tison*,],[*Jeffery et al.*(2011)*Jeffery, Hunke, and Elliott*,], and [*Saenz and Arrigo*(2012),]. The empirical approach of [*Cox and Weeks*(1988),] calculates desalination in growing ice as a combination of initial

salt entrapment, brine expulsion and gravity drainage. However, we know now from experiments and theory that both initial salt entrapment and brine expulsion do not desalinate the ice [*Notz and Worster*(2009),]. Both [*Vancoppenolle et al.*(2010) *Vancoppenolle, Goosse, de Montety, Fichefet, Tremblay, and Tison*,] and [*Jeffery et al.*(2011) *Jeffery, Hunke, and Elliott*,] treat gravity drainage as a diffusion caused by brine mixing, similar to turbulent mixing in boundary layers. However, both of these approaches are in contrast to studies of growing mushy layers which have shown that gravity drainage is a convective process linked to chimney formation [**?**, e.g.]]Tait1992,Chen1995,Wettlaufer1997,Notz2008. In sea ice, these chimneys are commonly referred to as brine channels. [*Saenz and Arrigo*(2012),] were the first to incorporate some limited convective aspects of gravity drainage into a 1D parametrization. However, the parametrization of [*Saenz and Arrigo*(2012),] relies heavily on empirical values, both to determine initial desalination and stable solid fractions.

We have developed two new one-dimensional parametrizations of gravity drainage; a *convective* parametrization and derived from it, a *simple* parametrization. The convective parametrization attempts to simulate brine movement as accurately as possible based on a few core assumptions. The simple parametrization is an attempt to produce a realistic salinity evolution at a lower computational cost.

3.1 Rayleigh number

Following previous studies [**?**, e.g.]]Tait1992,Wettlaufer1997, the onset and strength of gravity drainage in our parametrizations is linked to a porous-medium/mushy-layer Rayleigh number (R). In general, such a Rayleigh number describes the ratio of buoyancy to thermal diffusion in a porous medium. However, the specific formulations used vary considerably and are highly dependent on the assumed permeability. Due to this high variability in definitions, it is difficult to compare Rayleigh number values from different studies. A clear distinction should be made between Rayleigh numbers that represent the whole vertical sea-ice profile, and discretized local Rayleigh numbers that only represent a single horizontal layer. We use R^i to refer to the Rayleigh number of the layer i. As many of our assumptions are based on the results of [*Wells et al.*(2010) *Wells, Wettlaufer, and Orszag*,], we strive to keep our definition of the Rayleigh number qualitatively similar to their definition.

R^i can be regarded as the ratio of two representative timescales; the advective timescale t_D^i and the diffusive timescale t_A^i. The advective timescale is defined by the amount of time that the buoyancy driven brine in layer i needs to reach the ice-ocean interface. According to Darcy's law the brine moves at a speed of

$$v = \frac{g \triangle \rho \Pi}{\mu}$$

in which g is the gravitational acceleration, $\triangle\rho$ is the density difference between the brine and the underlying ocean water, μ the dynamic viscosity of the brine,

and Π the sea-ice permeability which is discussed in subsection 3.4. Accordingly, the time needed for brine to move the distance h^i from layer i to the ice-ocean interface equals

$$t_A^i = \frac{h^i \mu}{\tilde{\Pi}^i g \triangle \rho^i} \ .$$

Instead of the permeability of the layer i we use the minimal permeability of the layers beneath i,

$$\tilde{\Pi}^i = \min(\Pi^i, \Pi^{i+1}, ..., \Pi^n),$$

as the most impermeable layer acts as a bottleneck to the flow.

The diffusive timescale

$$t_D^i = \frac{(h^i)^2}{\kappa}$$

represents the diffusion time of thermal anomalies over the distance h^i for a given thermal diffusivity κ. For the thermal diffusivity $\kappa = k/(\rho c)$ we use the values of brine because due the small mass fraction of the displaced brine it represents the limiting factor keeping the brine and surrounding sea ice from reaching thermal equilibrium.

By computing density differences via the difference of brine salinity to the salinity of the lowest active layer n, $\triangle \rho^i = \rho_l \beta \triangle S^i = \rho_l \beta \triangle (S_{br}^i - S_{br}^n)$, the resulting Rayleigh number is

$$R^i = \frac{t_D^i}{t_A^i} = \frac{g \triangle \rho^i \tilde{\Pi}^i h^i}{\kappa \mu} = \frac{g \rho_l \beta \triangle S^i \tilde{\Pi}^i h^i}{\kappa \mu}.$$

A high Rayleigh number indicates that the moving brine flows quicker than thermal diffusion can enforce thermal equilibrium. As long as the moving brine is colder than the surrounding brine, it remains saltier and heavier and keeps descending. A low Rayleigh number indicates that thermal diffusion acts quicker than advection, returning the brine to thermal equilibrium and negating its buoyancy. Assuming both timescales are identical, brine in the ice would be brought into thermal (and salinity) equilibrium just as quick as it moves, resulting in a neutral buoyancy. This dependence of the convective strength on the Rayleigh number is the core of the convective parametrization we now turn to.

3.2 Convective parametrization

The convective parametrization strives to simulate the convective brine fluxes as accurately as possible. Our approach was heavily inspired by the 2D numerical studies of growing mushy layers conducted by [*Petrich et al.*(2004)*Petrich, Langhorne, and Sun*,] and [*Wells et al.*(2010) *Wells, Wettlaufer, and Orszag*,]. By assuming that chimney spacing in growing mushy layers maximizes potential energy transport, [*Wells et al.*(2010) *Wells, Wettlaufer, and Orszag*,] linked solute flux to the Rayleigh number of the convecting mushy layer. They concluded

that the solute flux increases approximately linearly with the Rayleigh number when the Rayleigh number is above a critical value. Below that value the circulation breaks down. Among the findings of a recent study of solute fluxes through chimneys by [*Rees Jones and Worster*(2012a),] is an analytically derived linear relationship of solute flux to Rayleigh number for 2D planar flows. [*Rees Jones and Worster*(2012a),] numerically extended their approach to 3D flows to discover some nonlinear behavior between solute flux and Rayleigh number. However, despite these nonlinear effects [*Rees Jones and Worster*(2012b),] still recommend parametrizing gravity drainage using a linear relationship of Rayleigh number to solute flux.

[*Wells et al.*(2010) *Wells, Wettlaufer, and Orszag*,] imitate a growing mushy layer with constant and well defined boundaries using a quasi-steady-state approach. As SAMSIM aims to simulate sea ice under all the variable conditions of the Arctic and Antarctic, our 1D parametrization must be able to deal with a much wider range of changing boundary conditions. We adopt their 2D results to a 1D parametrization using the following assumptions:

1. If the Rayleigh number of a layer is above a critical value, brine leaves the ice via brine channels into the underlying ocean.

2. The amount of brine leaving each layer i is proportional to $R^i - R_{crit}$.

3. All brine which leaves through channels is replaced by brine moving upward from the ocean.

4. Brine moving upward transports salt and thermal energy from layer to layer.

5. Brine leaving the sea ice downward through channels moves quickly enough that thermal interactions with the surrounding ice can be neglected.

Although we have strong support for all of these assumptions from 2D simulations and experiments, the more the conditions in the 1D model differs from the conditions simulated by [*Wells et al.*(2010) *Wells, Wettlaufer, and Orszag*,], the less confident we are in our assumptions. This is especially relevant for deep convection in thick ice. The first assumption implies that brine channels always exist when the Rayleigh number exceeds the critical value. Although this can be safely assumed near the ice-ocean interface, we have no evidence this assumption is always valid in thick ice. [*Cole and Shapiro*(1998),] found that brine channels typically extended 30 to 50 centimeters into 1.4 meter thick slices of first-year ice taken from two locations near Barrow. However, no channels were found that extended completely through the ice sheet. To truly validate or invalidate our assumption a much more thorough study of brine channels would be necessary.

The second assumption results in two free parameters, the critical Rayleigh number R_{crit} and a proportionality constant α which has the physical dimension of $kg/(m^3 s)$. How we estimate these parameters is described in section 4. This second assumption is not identical to the findings of [*Wells et al.*(2010) *Wells,*

Wettlaufer, and Orszag,], because [*Wells et al.*(2010) *Wells, Wettlaufer, and Orszag*,] linked the total brine flux to a non-local Rayleigh number and we link the brine flux of each layer to a local Rayleigh number. As no data or theory exists on how gravity drainage interacts with entrapped gas bubbles, our gravity drainage parametrization simply ignores the gas fraction.

Assumptions three and four are similar to those of [*Wells et al.*(2010) *Wells, Wettlaufer, and Orszag*,] and the channel-active-passive-zone model proposed by [*Rees Jones and Worster*(2012b),]. Figure 2 contains a sketch of the resulting brine and salt fluxes at the bottom of growing sea ice. In the sketch, the second to fourth lowest layers are equally unstable ($R^{n-1} = R^{n-2} = R^{n-3} > R_{crit}$) which leads to identical mass fluxes. The resulting heat fluxes would be opposite to the salt fluxes, with the warmer lower layers moving heat upward into the colder layers.

The model calculates the temperature, volume fractions and brine salinity of all active layers from 1 to n at the beginning of each time step according to equations (1), (2), and (3). Using those values the Rayleigh number of each layer (besides the lowest) is calculated. If $R^i > R_{crit}$ we consider the layer i convectively unstable. The mass of brine that flows from layer i ($br^i_\downarrow$) into the ocean in a time step of length dt is

$$br^i_\downarrow = \alpha(R^i - R_{crit}) \triangle z^i \cdot dt.$$

The downward flowing brine is scaled by the time step dt and the layer thickness $\triangle z$, and has the temperature and salinity of the layer it originated from. After $br_\downarrow$ has been computed for all layers, the resulting upward brine fluxes from layer $i+1$ to layer i resulting from mass conservation are

$$br^i_\uparrow = \sum_{k=1}^{k=i} br^k_\downarrow = br^{i-1}_\uparrow + br^i_\downarrow$$

The amount of brine entering the layer i from below is $br^i_\uparrow$ which equals the sum of brine leaving that layer. Since we advect salt with the upstream method, the amount of salt which enters the layer i per time step is $br^i_\uparrow \cdot S^{i+1}_{br}$ and the amount of salt leaving the layer i is $(br^{i-1}_\uparrow + br^i_\downarrow) \cdot S^i_{br}$. The resulting change in absolute salinity is

$$\triangle S^i_{abs} = br^i_\uparrow \cdot S^{i+1}_{br} - (br^{i-1}_\uparrow + br^i_\downarrow) \cdot S^i_{br} = br^i_\uparrow \cdot (S^{i+1}_{br} - S^i_{br}).$$

This convective parametrization requires a relatively small time step, especially since the bottom layers of SAMSIM are relatively thin. In this paper the bottom layers vary from 2 mm to 5 cm. A basic numerical rule of thumb for 1D advection is that the distance traveled by the fluid per time step should not be larger than a tenth of the grid spacing. Translated to SAMSIM this rule states that the volume of brine moving from layer to layer per time step should not be larger than a tenth of the brine volume in those layers. The brine volume of each layer and the flow are extremely variable, so a relatively small time step is necessary to avoid numerical instabilities. Although a simple flux correction

is implemented to ensure that the salt advection remains positive definite, the computational cost of the stand alone model is small enough that we can chose the time step to be as small as we need.

3.3 Simple parametrization

The convective parametrization is ill-suited for earth system models as it requires a small time step to avoid instabilities. As an alternative we propose a simpler parametrization as a tool to improve sea-ice thermodynamics and salt release into the ocean for climate models. In this paper we refer to the simpler salinity parametrization as the simple parametrization and to the more complex parametrization that calculates brine fluxes as the convective parametrization.

The simple parametrization is based on the assumption that convectively unstable layers lose salinity until they are stable. This assumption is a simplification of the convective parametrization in which convectively unstable layers lose salt through convection. Instead of losing salt via convection, the simple parametrization directly reduces the amount of salt in the layer until the layer is stable. The simple parametrization always produces a stable salinity profile while the convective parametrization slowly evolves towards a stable salinity profile.

The first step of the simple parametrization is identical to the convective parametrization, the Rayleigh numbers of all layers are calculated. If the Rayleigh number is higher than the critical value, the layer is considered convectively unstable. But instead of calculating brine fluxes and resulting salt transport, in the simple parametrization we reduce the salinity by a certain fraction. So if $R^i > R_{crit}$, then the salinity will be multiplied with a fixed constant $\gamma < 1$ leading to S^i_{abs} in the following time step being γS^i_{abs}. The resulting parametrization is unconditionally stable and can be summarized in the following line:

$$\textit{If: } R^i > R_{crit} \qquad \textit{Then: } S^i_{abs} = \gamma S^i_{abs}$$

Again we have a parametrization with two free parameters: R_{crit} and γ. For R_{crit} we use the same value as the convective parametrization. γ must have a value between 0 and 1. The closer γ is to 1 the smoother the salinity evolution, but γ must be small enough to ensure that the salinity decreases faster than the surrounding ice conditions evolve. The smaller the time step, the closer γ can be to 1. We recommend keeping γ above 0.9, as large jumps in salinity lead to sudden temperature changes. Our experience indicates that slight changes of γ do not affect the results much.

We expect the largest differences between the two schemes to occur when sea ice grows rapidly, because the simple parametrization forces the salinity profile into equilibrium much quicker than the brine circulation of the convective parametrization. Another difference is that a convectively stable layer below unstable layers can desalinate in the convective parametrization, but not in the simple parametrization.

3.4 Permeability

In porous media, permeability is part of the proportionality constant in Darcy's law which relates flow rate to a pressure gradient. In contrast to static materials (such as sandstone) the permeability of sea ice is continuously evolving and is affected by temperature, ice structure, salinity, and flow direction. Brine movement in sea ice causes heat and salt transport, which leads to a change in permeability, which in turn affects the brine movement. This behavior leads to highly non-linear effects which can be exceedingly difficult to capture in numerical models.

The permeability of sea ice is an extremely complex ongoing research topic which has been studied extensively [**?**, e.g.]]Petrich2006,Golden2007,Pringle2009,Buettner2011,Jones2012. In SAMSIM we define permeability as an empirical function of the fluid volume fraction. This commonly used approach neglects the ice structure, which seems justified for our purposes because [*Gough et al.*(2012) *Gough, Mahoney, Langhorne, Williams, and Haskell*,] concluded that desalination processes are mostly unaffected by the ice structure.

All tests in this paper were conducted using the relationship proposed by [*Freitag*(1999),]:

$$\Pi^i(\phi_l^i) = 10^{-17}(10^3\phi_l^i)^{3.1}.$$

We believe this empirically derived relationship is similar enough to the $\Pi = \Pi_0(\phi_l)^3$ used by [*Wells et al.*(2010) *Wells, Wettlaufer, and Orszag*,] to avoid issues when transferring the results of [*Wells et al.*(2010) *Wells, Wettlaufer, and Orszag*,] to SAMSIM.

It is well known that at low liquid fractions sea-ice can become impermeable, and $\phi_{l_{crit}} = 0.05$ is often used as threshold value under which the remaining brine pockets are assumed to be isolated from each other [**?**, e.g]]Golden1998,Petrich2006,Golden2007,Vancoppen As SAMSIM attempts to represent a spatial average of possibly highly heterogeneous sea-ice, we believe that small permeabilities at low liquid fractions are justifiable. Also, if a low permeability results in a Rayleigh number below R_{crit}, our gravity drainage parametrizations predict no changes. So as long as $R < R_{crit}$, it is irrelevant if the ice is truly impermeable or not.

4 Parameter estimation and evaluation

The convective parametrization introduced in subsection 3.2 contains two free parameters, the dimensionless R_{crit} and α with the physical dimension of $kg/(m^3 s)$. In this section we detail how we derived α and R_{crit} from laboratory salinity measurements, and how we determined that both parameters are independent of the vertical resolution of the model.

4.1 Salinity measurements

The salinity measurements we use stem from a laboratory experiment that was described in section 8.4 of [*Notz*(2005),]. In this experiment, an NaCl solution was cooled from above by a cooling plate that was switched from $-5°$ to $-10°$ C every 12 hours. The ice grew to almost 15 cm over the 72 hours of the experiment, which was repeated once under identical conditions. Throughout the experiment, salinities were measured in situ at fixed depths at a high temporal resolution using a so-called wireharp [*Notz and Worster*(2008),].

The three sub panels of figure 3 show salinity measurements at three points in time. To what extent the differences between the two experiment repetitions (one marked by black dots, the other by white dots) are due to measurement errors or actual physical differences is impossible to tell. [*Cottier et al.*(1999)*Cottier, Eicken, and Wadhams*,] showed that growing sea ice can have a high horizontal gradient in salinity linked to the location and morphology of the brine channels. We assume that the experiments were conducted under identical conditions and the differences result from the sampling size of ice between the wires and measurement errors.

We choose this experiment for multiple reasons. The first, and arguably the most important reason, is the high spatial resolution of the data. Also of great advantage is that the experiment was conducted twice, and that the controlled environment of the experiment can be easily translated to boundary conditions for the model. In contrast, field studies of sea ice contain many unknowns, such as precise heat fluxes and dynamic effects, which makes field measurements difficult to reproduce with a high degree of accuracy.

The final reason for using this experiment is that the temperature of the cooling plate alternated between -5° and -10° C. Our convective parametrization is based on the results of [*Wells et al.*(2010) *Wells, Wettlaufer, and Orszag*,], in which a steady cooling temperature was assumed. If SAMSIM can reproduce the experiments, we have shown that our approach can deal with more complex conditions than those of [*Wells et al.*(2010) *Wells, Wettlaufer, and Orszag*,].

A limitation of the data is the rather short duration of the experiment. Also, the experiment would ideally have been conducted more than twice.

4.2 Parameter optimization

We use the Levenberg-Marquardt algorithm to determine the optimal values of α and R_{crit} [*Levenberg*(1944),]. The metric the algorithm seeks to minimize is the difference between the measured and model salinity every twelve hours. If a measurement lies inside a model layer, it is directly compared to that layer. If the measurement lies between two layers, it is compared against an average of those two layers.

We optimize the parameters separately for the first and second experiments measured by [*Notz*(2005),]. To ensure that the optimization results are not local minima, we chose four different initial estimations of α and R_{crit}. All four initial values result in almost identical values for all the data sets, which

is by itself a promising sign (figure 4a). The differences resulting from using other initial values are smaller than the precision criterion required to stop the algorithm. The two parameters vary by roughly a factor of two from set 1 (α=$1.93 \cdot 10^{-3} kg/(m^3 s)$, R_{crit}=0.67) to set 2 (α=$1.28 \cdot 10^{-3} kg/(m^3 s)$, R_{crit}=1.48).

To get an indication of how sensitive the parameters react to different values, we create an additional artificial data set by averaging the two experiments (figure 4a). The average of both data sets leads to values in between the two previous results (α=$1.56 \cdot 10^{-3} kg/(m^3 s)$, R_{crit}=1.01) which we use as the default setting for SAMSIM.

4.3 Resolution dependency

To test the dependency of the parameters to the vertical resolution we conducted a simulation with a reference run at a vertical grid spacing of 1 cm, in which ice was grown from a NaCl solution at a fixed cooling temperature over 6 days. A relatively high salinity of 70 ppt was chosen to increase the strength of gravity drainage and the resulting freshwater signal. Every 12 hours the freshwater content of all layers was saved. The Levenberg-Marquardt algorithm was used to optimize the model with different vertical resolutions to reach the same total freshwater content each 12 hours. In contrast to the previous subsection in which the salinity profile was used to determine the model performance, we choose to compare the freshwater content instead as it is difficult to compare profiles at different resolutions. We also choose to keep the cooling temperature steady to ensure a linear temperature profile, which minimizes thermodynamic differences due to the changing resolution.

The spacing of the model varied from 2 mm to 2 cm in steps of 1 mm, a range that covers most of the values used in this paper. We find that the variations of α and R_{crit} are smaller than 10 % and show no trend (figure 4b). From this we conclude that our parameters α and R_{crit} —which we determined using a 2 mm grid— do not seem to depend on resolution and are valid for vertical resolutions up to at least 2 cm .

4.4 Parametrization evaluation

Although we have determined our free parameters by optimizing the model using salinity measurements, this in no way guarantees that the model results reproduce the measurements. To evaluate the parametrization we compare the resulting salinity profiles of the model for the different values of α and R_{crit} against the measurements (figure 3). The model output generally agrees very well with measurements, with almost all deviations being smaller than the measured uncertainty. This good agreement indicates that the assumptions on which our convective parametrization is based are valid for these conditions. Additionally, SAMSIM proves itself capable of reproducing the thermodynamics of the experiment.

We can not verify if the high salinity values directly at the cooling plate predicted by the model occurred during the experiments. But it is to be expected that the ice crystal formation at the beginning of the experiment includes crystalline processes which can not be captured using mushy layer theory. It is also difficult to keep the cooling plate at a constant negative temperature when initially brought in contact with the NaCl solution because of the very rapid initial exchange of latent heat. The resulting initial temperature fluctuations are not included in the boundary conditions of the model simulations.

It is remarkable that despite the rather large spread of α and R_{crit} the model setups 1, 2, and 1+2 behave very similar. This similar behavior can be attributed to two causes. Firstly, from the formulation of the brine fluxes in the convective parametrization, namely flow equals $\alpha \cdot (R - R_{crit})$, it follows that α and R_{crit} have opposing effects. The values determined by the optimization are balanced against each other (high R_{crit} and low α, or vice-versa), resulting in a similar flow strength. The second cause is that gravity drainage is a relatively stable process. Increased convection leads to increased salt loss, which results in lower liquid fractions and permeability, which in turn reduces convection. Slow convection leads to ice with a higher permeability, which leads to increased convection.

In conclusion, we derived estimations of α and R_{crit} which are independent of grid resolution. More data from longer experiments is needed to further improve the estimations of α and R_{crit}, which are highly dependent on the assumed permeability. Using these values of α and R_{crit} in the convective parametrization enables the model to reproduce measured salinity profiles.

5 Idealized tests

After developing, tuning, and evaluating our convective gravity drainage parametrization with small-scale laboratory data, we now study gravity drainage under various idealized conditions. The tests with idealized boundary conditions are used to study the depth and strength of gravity drainage, to quantify the desalination caused by gravity drainage, and to investigate the relationship between growth speed and the final bulk salinity of sea ice. The conclusions we draw from the idealized test cases are then tested under more realistic conditions in the next section, in which we force SAMSIM with reanalysis data.

5.1 Constant cooling

Our first test case is the freezing of a NaCl solution from a constant cooling temperature, which is the most often used setup for laboratory studies [**?**, e.g.]]Tait1992,Chen1995,Wettlaufer1997,Notz2009.

We conduct simulations of a NaCl solution freezing at four different cooling temperatures ranging from -5° to -35° C to cover the full range of growth speeds which occur in the Arctic and Antarctic. For these tests SAMSIM's grid is set to N_{top}=5, N_{mid}=10, N_{bot}=10, and $\triangle z_0$=1.0 cm with a time step of 5 s. We

wait until the ice grows to a thickness of 50 cm and then compare the resulting profiles of salinity, solid fraction and Rayleigh number. These test cases provide a frame of reference on how the bulk salinity of sea ice is related to growth speed.

We find that more salt is retained in the ice the colder the cooling temperature (figure 5a), as was also found in the laboratory experiments of [*Cox and Weeks*(1975),] and [*Wettlaufer et al.*(1997) *Wettlaufer, Worster, and Huppert*,]. Based on the salinity profiles, we conclude that a layer of growing sea ice can not retain more than 10 ppt salt once convection has ceased.

Despite the higher salinity, the colder experiments have a slightly higher solid fraction (figure 5b). This can easily be understood: because the colder experiments have higher brine salinities, the permeability must be smaller than in the warmer experiment to inhibit convection and retain salt. In all simulations almost all the convection occurs in the lowest 10 cm regardless of growth speed (figure 5c).

The Rayleigh number of the slower-growing ice remains close to the critical value of 1.01 in the top 40 cm of the ice, while the faster-growing ice is more stable there. In contrast, the faster-growing ice is much more unstable in the lowest 10 cm. All simulations remain slightly unstable in the top 5 cm, driving a very weak circulation over the complete 50 cm. This top instability is maintained by the constant surface temperature. Slight fluctuations in this temperature would remove the instability.

To summarize these results, we find that slow growing warm ice desalinates stronger and results in a marginally stable Raleigh number profile. In contrast, faster-growing colder ice retains more salt, and the ice becomes convectively stable once gravity drainage ceases. As almost all convection occurs in the lowest 10 cm, we conclude that multiple layers in the lowest 10-20 cm are necessary to properly simulate gravity drainage numerically. The relationship of higher salinity for fast growth speed and lower salinity for lower growth speed was also found in laboratory experiments by Cox and Weeks (1974). These experiments were used to derive a fractionation coefficient based on growth velocity that describes the incorporation of salt into the advancing front. However, our results confirm the findings of Notz and Worster (2009) that such fractionation coefficient does not reflect the underlying physics of the measured relationship between growth speed and sea-ice bulk salinity. We will further examine this relationship for more realistic boundary conditions in section 6.1.

5.2 Warming triggered convection

It is currently unclear if gravity drainage can occur in warming sea ice. Measurements of salt fluxes below sea ice [*Widell et al.*(2006) *Widell, Fer, and Haugan*,] and of algae behavior in sea ice during autumn [*Fritsen et al.*(1994) *Fritsen, Lytle, Ackley, and Sullivan*,] indicate that convection may occur, as do recent observations of short-lived salinity anomalies under warming sea ice (*Jardon et al., Full-depth desalination of warm sea ice, submitted manuscript*). In this subsection we introduce an experiment designed to test if it is possible to trigger

gravity drainage in sea ice by warming the ice from above and/or below. A secondary goal is to study how gravity drainage affects the sea ice.

In principle, warming sea ice can lead to gravity drainage by increasing the permeability of the ice. Also, melting at the ice-ocean boundary can increase the buoyancy of the brine. The buoyancy is increased by the reduction of the salinity below the ice caused by melting ice at the ice-ocean boundary. Assuming the brine salinity in the sea ice remains steady, fresher water below the ice creates a larger density difference.

To maximize our chance of triggering convection we create initial conditions which are just stable. These initial conditions are reached by growing ice from a fixed temperature of -16.7° C from salt water with a salinity of 34 ppt. The sea ice grows until it reaches a thickness at which the prescribed ocean heat flux of 20 W balances the growth. Over the roughly 18 months simulated to reach the equilibrium state, gravity drainage slowly desalinates the ice until the Rayleigh numbers are just below the critical value.

Three different experiments were applied using the stable initial conditions to trigger deep convection. Experiment I raises the top temperature from -16.7° C to -5° to increase permeability while reducing buoyancy. Experiment II increases the oceanic heat flux from 20 to 100 W to increase buoyancy by melting ice at the ice-ocean boundary. Experiment III is a combination of the atmospheric and the oceanic forcing in experiments I and II.

All three experiments succeeded to trigger convection in SAMSIM, with each experiment resulting in different convection patterns and salinity profiles (figure 6). Experiment I mostly destabilizes the upper half of the ice (figure 6-I-C), but the strongest desalination occurs in the bottom half of the ice (figure 6-I-B). The increased oceanic heat flux of forcing II destabilizes the lowest 50 cm and the top 10 cm (figure 6-II-C). The desalination caused in experiment II is weaker than the desalination of experiment I and is mostly confined to the lowest 40 cm (figure 6-II-B). This desalination caused by an increased oceanic heat flux is possibly what was observed by [*Widell et al.*(2006) *Widell, Fer, and Haugan*,], who linked salt release to upward oceanic heat fluxes.

The convection and desalination results of experiment III can roughly be described as an accelerated linear combination of the convection and desalination of experiment I and II. The resulting desalination is strong enough that it leads to a visible warming in the lower 40 cm after four days, as the ice solidifies and warms at the same time (figure 6-III).

From these three experiments we conclude that gravity drainage can occur during top warming and bottom melt under ideal conditions. Warming the ice from above creates a stronger effect than dissolving the ice from below, and a combination of both leads to the strongest effects. In contrast to the gravity drainage that occurs during growth, the resulting deeper convection can span the whole ice layer. The desalination caused by the deep convection is strongest in the lower half.

In nature, atmospheric and oceanic forcing could easily be as strong or stronger than the idealized forcings we used in this experiment. However, it is highly unlikely that the initial ice conditions of the idealized experiments

occur naturally. From these two statements we conclude that deep convection is possible in reality, but the resulting convection will likely be weaker than in the idealized experiments. The desalination of the lower half of sea ice after the onset of flushing, which was already noted by [*Malmgren*(1927),] and [*Holt and Digby*(1985),], could be the result of such warming-induced deep convection.

6 Seasonal growth under reanalysis forcing

To examine how gravity drainage occurs under more realistic conditions, we conduct a case study of a single growth season using reanalysis data. We use this test case to determine which of our results from the idealized tests (such as those concerning deep convection and the link between growth speed and final salinity) are also valid under realistic conditions (subsection 6.1). This test case is also used to compare the simple against the convective gravity drainage parametrization and to quantify the effect of gravity drainage on the thermal properties of sea ice (subsections 6.2 and 6.3).

To force SAMSIM with reanalysis data, the surface temperature is derived by balancing outgoing long wave radiation with three-hourly ERA-interim fluxes. Both the fluxes and precipitation were taken from a grid point close to where the SHEBA campaign was conducted [*Perovich et al.*(1999),], namely at 75 N and 217.5 E. We randomly chose the year 2005 to simulate the total growth season from ice formation to maximum thickness. As we have no reanalysis data of oceanic heat fluxes we approximate the oceanic heat flux as a simple sine curve with a period of 1 year, which is based loosely on the values [*Huwald et al.*(2005b)*Huwald, Tremblay, and Blatter*,] derived from the SHEBA measurements. The oceanic heat flux reaches 14 W/m^2 in Autumn and sinks to 0 W/m^2 in Spring. For SAMSIM's grid we choose N_{top}=10, N_{mid}=40, N_{bot}=20, and $\triangle z_0$=1.0 cm to highly resolve the bottom 20 cm of the ice. To avoid numerical issues in these small layers we use a time step of 10 seconds. Aspects we neglect in this simulation are the initial formation of frazil ice and the feedbacks of the sea ice on oceanic, sensible, and latent heat fluxes.

To determine if the model output is realistic, we evaluate the test case against data from the SHEBA Baltimore site and against the empirical relationship of [*Kovacs*(1997),]. Our model produces a similar dependence of mean bulk salinity on ice thickness as given by the empirical function of [*Kovacs*(1997),] (figure 7). In thin ice, modeled bulk salinity is slightly higher, which could also be related to the outflow of brine and hence an underestimate of sampled bulk salinity in thin sea ice.

A casual comparison with buoy data of first year ice from the SHEBA Baltimore site shows a good general agreement between simulated and measured temperature profiles [**?**, not shown]]Perovich2012. In the case study, the model grows 1.8 m of ice and accumulates approximately 30 cm of snow (figure 8). The model is somewhat thicker than the maximum thickness of 1.5 m measured at the Baltimore site, but the Baltimore site is likely somewhat thinner due to the thicker snow cover of 50 cm compared to the 30 cm of snow in our case

study. From the general similarities of the model with the SHEBA data and the empirical salinity-thickness relationship of [*Kovacs*(1997),] we conclude that the model results fulfill basic expectations.

6.1 Gravity drainage under reanalysis forcing

The high spatial and temporal resolution of the case study simulation supplies a wealth of information on how gravity drainage, salinity, and temperature interact (figure 8). From this data we draw conclusions on the depth and variability of gravity drainage, the salinity evolution in growing sea ice, how gravity drainage responds to temperature, and how salinity is linked to growth speed.

From the blue line in subfigure 8c we can see that although gravity drainage occurs mostly in the lowest 20 cm, there is a great amount of variation. Not only does the convection depth at the bottom vary, but also additional layers separated from the lower convection become unstable now and then. Most notable is the full depth convection after six months when top warming destabilizes the top 50 cm of ice. Similar events of smaller magnitude occur shortly after two months and after roughly three and a half months. This variance of gravity drainage is not a simple reaction to temperature forcing or random model behavior. Instead, this variance results from the complicated interplay of salinity, buoyancy, and permeability.

Comparing the 6 ppt salt contour of subfigure 8b to the blue line of subfigure 8c shows that the 6 ppt contour roughly outlines the lower convective ice layers. The 6 ppt contour shows a stepwise shape at approximately 1.2, 1.6, 2.2, 3.3, 5.2, and 6 months. These steps all coincide with a warming of the ice, as can be seen in subfigure 8a. At the same time, the depth of gravity drainage increases for a short time and then collapses. From this behavior we conclude that gravity drainage reacts in cycles to the temperature evolution. The cycle begins when the surface temperature drops and ice grows faster at the ice-ocean boundary. While the ice continues to grow, the newly formed ice remains convectively unstable. At some point in time the surface temperature rises again. As the ice warms, the convection depth increases or remains constant. When the ice once again begins to cool, most of the convectively unstable regions stabilize and the cycle repeats itself. Such a cycle in figure 8 begins shortly before and ends slightly after two months, during which the top temperature drops from above -5° C to below -20° C and returns above -10° C.

We will now turn to comparing these results to those from the idealized test case described in section 5. Doing so, it is interesting to note that in the simulation under realistic forcing, gravity drainage reduces the salinity to a stable value below 6 ppt. This value of 6 ppt lies below the upper threshold of 10 ppt which we determined from idealized experiments in section 5 to be the absolute maximum salinity possible in stable sea ice. In addition, the link between faster growth speed and higher salinity that we found in section 5 no longer holds: Such link would result in a nonlinear relationship of salt flux to growth rate, which we do not find for the realistic forcing (figure 9). We believe that the cyclic interaction of temperature and convection discussed in the above

paragraph both disrupts the link between growth speed and salinity and causes a reduced stable bulk salinity.

In section 5 we concluded from idealized experiments that top warming can lead to gravity drainage over the whole ice layer. We also concluded that such convection would lead to a desalination which is strongest in the lower ice layers. The full depth convection which occurs after six months in the reanalysis-forced test case shows that both of these conclusions still hold for realistic boundary conditions. The resulting desalination is clearly visualized by the 3 ppt contour of salinity (subfigure 8b). Comparing the 2.5 % contour (subfigure 8c) before and after the event highlights the reduction in liquid fraction caused by the desalination.

6.2 Convective versus simple parametrization

To study how closely the simple parametrization (introduced in subsection 3.3) mimics the convective parametrization we compare salinity profiles resulting from both parametrizations for the reanalysis-forced case study. As the simple parametrization is intended for use in coupled models in which using 70 levels is unthinkable, we also run SAMSIM at a lower resolution for this analysis. For the high-resolution case, we chose N_{top}=10, N_{mid}=40, N_{bot}=20, and $\triangle z_0$=1.0 cm (figure 10a). The low-resolution is based on N_{top}=3, N_{mid}=3, N_{bot}=4, and $\triangle z_0$=5 cm (figure 10b).

The simple convection provides a reasonable salinity profile approximation, especially at low resolution (figure 10). Although the convective parametrization desalinates growing sea ice somewhat slower, the differences are rather small. Two characteristics of the high resolution convective parametrization are not reproduced by the simple parametrization: the high salinity in the top layer, and the desalination caused by deep convection after six months. The high salinity in the top layer can not be reproduced by the simple parametrization because it has no sense of the speed of desalination and stabilizes the salinity profile almost immediately. The deep convection can not be captured by the simple parametrization as it arises from the convective nature of gravity drainage.

6.3 Relevance to climate models

In this subsection we seek to quantify how relevant gravity drainage is for climate models. To achieve this, we compare the reanalysis-forced simulations with the convective and simple parametrization against simulations without gravity drainage. Due to their relevance in climate models we choose to evaluate ice thickness, enthalpy, thermal resistance, and freshwater column.

The salinity of the comparison runs are determined by the initial salinity, which we set to 4 or 7 ppt. However, setting an initial salinity is not identical to the constant salinity approach often used in front tracking models. The most significant difference is that the freezing temperature at the ice-ocean interface changes as well, which leads to ice forming sooner in open water. Also, brine expulsion redistributes small amounts of salt.

In the rest of this subsection we will refer to the run using the full convective parametrization as the convec run, the run using the simple parametrization as the simple run, and the runs without gravity drainage as 4 and 7 ppt run in reference to their initial salinities. The same terminology is used in figure 11.

As expected, the 4 and 7 ppt runs produce thicker ice than the full convective run, in part owing to the higher freezing temperature and the higher thermal conductivity of fresher ice (figure 11a). The simple parametrization lies between the convec and constant salinity runs, which we attribute to the simple run desalinating quicker than the convec run while maintaining the 34 ppt at the ice-ocean interface.

To study both short-term variations and long-term trends of the evaluated quantities, we subtract the running monthly mean of the convec run from all four runs. These differences are then smoothed by a weekly running average and plotted in subfigure b to e of figure 11. The short-term variations of all runs agree well with two exceptions. The first exception occurs during ice formation because the constant salinity runs freeze sooner and quicker. The second exception is visible in subfigure 11e after six months when the deep convection occurs. Only the convec run shows a short-term freshening.

At the end of the growth season all evaluated quantities of the simple run are approximately 4 % higher than the convec run. Although the 4 and 7 ppt runs have a similar thickness, the 4 ppt run's thermal resistivity is in better agreement with the convec run. In contrast, the enthalpy and fresh water column of the 7 ppt run agree better than the 4 ppt run with the convec run. This shows that although the initial salinity can be varied to fit one quantity, no value can fit all. At the end of the growth season the average of all quantities over both the 4 and 7 ppt run is approximately 7 % higher than the convec run.

7 Summary & Discussion

7.1 Summary

In this paper we have studied gravity drainage using a convective parametrization with two free parameters, the critical Rayleigh number and a proportionality constant α. Values for these two parameters were determined using the Levenberg-Marquadt optimization algorithm and salinity measurements from laboratory experiments. The optimization results were robust against changes in the initial values but the uncertainties should be reduced with more data, especially from longer experiments. Our derived value of the critical Rayleigh number (1 ± 0.5) agrees well with theoretical expectations but is difficult to compare to the value of 5 used by [*Vancoppenolle et al.*(2010) *Vancoppenolle, Goosse, de Montety, Fichefet, Tremblay, and Tison*,] or the values of 0.5-2 which [*Gough et al.*(2012) *Gough, Mahoney, Langhorne, Williams, and Haskell*,] derived from ice-core measurements because slightly different definitions of the Rayleigh number were used. [*Vancoppenolle et al.*(2010) *Vancoppenolle, Goosse, de Montety, Fichefet, Tremblay, and Tison*,] and [*Gough et al.*(2012) *Gough,*

Mahoney, Langhorne, Williams, and Haskell,] both use the thermal diffusivity of sea ice which is highly temperature and salinity dependent instead of the thermal diffusivity of brine we use in our definition of the Rayleigh number [*Schwerdtfeger*(1963),].

The link between growth speed and resulting bulk salinity as indicated from laboratory experiments [*Cox and Weeks*(1975), *Wettlaufer et al.*(1997) *Wettlaufer, Worster, and Huppert*,] and field studies [*Gough et al.*(2012) *Gough, Mahoney, Langhorne, Williams, and Haskell*,] is simulated by SAMSIM for sea ice growing from a fixed surface temperature. In contrast to the findings of these measurements, comparing salt release versus growth rate of a reanalysis-forced test case shows no indication that more salt is retained at faster growth speeds. We believe that the strong temperature variations of the test case and the resulting destabilization of stable layers disrupt the link between growth speed and resulting bulk salinity.

We show that SAMSIM allows for deep convection in sea ice, and deep convection can be found in both idealized and more realistic runs. The strongest salinity signal from deep convection is found in the lower and middle ice layers, which could explain observations of desalination near the ice-ocean interface during the melt season [*Malmgren*(1927), *Holt and Digby*(1985),]. However, all results related to deep convection are somewhat speculative because deep convection is very sensitive to various model assumptions (e.g. permeability) and no direct measurements are available to compare SAMSIM's results against reality. We also show that under idealized conditions a freshening of the water directly under the ice caused by an increased oceanic heat flux can lead to gravity drainage near the ice-ocean interface. This mechanism could explain the link between salt flux and oceanic heat measured in the field by [*Widell et al.*(2006) *Widell, Fer, and Haugan*,].

We compared a model run using the full convective gravity drainage parametrization against runs with fixed salinities and showed that the total enthalpy, thermal resistance, and freshwater column differ significantly over the growth season ($\approx$ 7 % higher all together) but have similar short-term variations. Only at ice formation and during deep convection —the processes most difficult to reproduce correctly in a 1D model— does model behavior diverge. As gravity drainage is the dominant but not sole desalination processes in sea ice, the effect of the total salinity evolution has yet to be assessed. Also, since the ocean and incoming atmospheric heat fluxes were prescribed, possible feedbacks were not included in this study.

As a computationally cheap alternative to the convective parametrization we also developed an unconditionally stable and numerically cheap parametrization referred to as the simple parametrization. It is based on the assumption that the salinity profile evolves to reduce convective instability. The simple parametrization is capable of reproducing the general salinity profile of the convective parametrization and leads to an approximately 4 % overestimation of total enthalpy, thermal resistance, and freshwater column.

7.2 Discussion

Simplified sea-ice models with few layers (such as those proposed by [*Semtner*(1976),] and [*Winton*(2000),]) are unlikely to benefit from a gravity drainage parametrization as the parametrizations require a meaningful vertical temperature and salinity profile. Additionally, the possible improvements are relatively small compared to the model limitations [*Wilkins*(2010),]. [*Massonnet et al.*(2011)*Massonnet, Fichefet, Goosse, Vancoppenolle, Mathiot, and Beatty*,] stated that a correct brine representation could improve the effects of the ice thickness distribution by increasing melt. We believe that more complex sea-ice models which have multiple vertical layers and many ice thickness categories (e.g. CICE, LIM) could profit from the inclusion of gravity drainage. Recently, a scheme similar to the one described here was successfully implemented into CICE *(*A. Turner et al., title, manuscript in preparation). Earth system modelers looking to include the salinity evolution into their sea-ice model could profit from the implementation of our simple gravity drainage parametrization, which due to its unconditional numerical stability and low time step requirements is well suited to the task. For researchers conducting detailed process studies of biogeochemistry and thermodynamics the full convective gravity drainage parametrization that we introduced can provide a high quality estimation of brine fluxes.

acknowledgments

We would like to thank Juan Pedro Mellado and David Rees Jones for helpful comments on previous versions of this paper. Andrew Wells, Martin Vancoppenolle, and Christopher Petrich all provided ideas and advice during the early stages of our research for which we are grateful. We would also like to thank the ECMWF for providing ERA-interim reanalysis data and the University of Chicago for releasing MINPACK.

References

[*Bitz and Lipscomb*(1999)] Bitz, C. M., and W. H. Lipscomb (1999), An energy-conserving thermodynamic model of sea ice, *J. Geophys. Res.*, *104*(C7), 15,669–15,677, doi:10.1029/1999JC900100.

[*Büttner*(2011)] Büttner, J. (2011), Permeability of young sea ice from micro-tomographic images, Master's thesis, Geophysical Institute, University of Bergen, Bergen, Norway.

[*Chen*(1995)] Chen, C. F. (1995), Experimental study of convection in a mushy layer during directional solidification, *J. Fluid Mech.*, *293*, 81–98, doi: 10.1017/S0022112095001649.

[*Cole and Shapiro*(1998)] Cole, D. M., and L. H. Shapiro (1998), Observations of brine drainage networks and microstructure of first-year sea ice, *J. Geophys. Res.*, *103*(C10), 21,73921,750.

[*Cottier et al.*(1999)*Cottier, Eicken, and Wadhams*] Cottier, F., H. Eicken, and P. Wadhams (1999), Linkages between salinity and brine channel distribution in young sea ice, *J. Geophys. Res.*, *104*(C7), 15,859–15,871, doi: 10.1029/1999JC900128.

[*Cox and Weeks*(1975)] Cox, G., and W. Weeks (1975), Brine drainage and initial salt entrapment in sodium chloride ice., *Tech. rep.*, DTIC Document.

[*Cox and Weeks*(1988)] Cox, G. F. N., and W. F. Weeks (1988), Numerical simulations of the profile properties of undeformed first-year sea ice during the growth season, *J. Geophys. Res.*, *93*(C10), 12,449–12,460, doi: 10.1029/JC093iC10p12449.

[*Feltham et al.*(2006)*Feltham, Untersteiner, Wettlaufer, and Worster*] Feltham, D. L., N. Untersteiner, J. S. Wettlaufer, and M. G. Worster (2006), Sea ice is a mushy layer, *Geophys. Res. Lett.*, *33*(14), L14,501, doi:10.1029/2006GL026290.

[*Freitag*(1999)] Freitag, J. (1999), The hydraulic properties of arctic sea ice - implications for the small scale particle transport (in german), *Berichte zur Polarforschung*, *325*.

[*Fritsen et al.*(1994)*Fritsen, Lytle, Ackley, and Sullivan*] Fritsen, C. H., V. I. Lytle, S. F. Ackley, and C. W. Sullivan (1994), Autumn bloom of antarctic pack-ice algae, *Science*, *266*(5186), 782784.

[*Golden et al.*(1998)*Golden, Ackley, and Lytle*] Golden, K., S. Ackley, and V. Lytle (1998), The percolation phase transition in sea ice, *Science*, *282*(5397), 22382241.

[*Golden et al.*(2007)*Golden, Eicken, Heaton, Miner, Pringle, and Zhu*] Golden, K. M., H. Eicken, A. L. Heaton, J. Miner, D. J. Pringle, and J. Zhu (2007), Thermal evolution of permeability and microstructure in sea ice, *Geophys. Res. Lett.*, *34*(16), L16,501, doi:10.1029/2007GL030447.

[*Gough et al.*(2012)*Gough, Mahoney, Langhorne, Williams, and Haskell*] Gough, A. J., A. R. Mahoney, P. J. Langhorne, M. J. M. Williams, and T. G. Haskell (2012), Sea ice salinity and structure: A winter time series of salinity and its distribution, *J. Geophys. Res.*, *117*(C3), C03,008.

[*Gu et al.*(2012)*Gu, Lin, Xu, Yuan, Tao, Li, and Liu*] Gu, W., Y. Lin, Y. Xu, S. Yuan, J. Tao, L. Li, and C. Liu (2012), Sea ice desalination under the force of gravity in low temperature environments, *Desalination*, *295*(0), 11–15.

[*Holt and Digby*(1985)] Holt, B., and S. A. Digby (1985), Processes and imagery of first-year fast sea ice during the melt season, *J. Geophys. Res.*, *90*(C3), 5045–5062, doi:10.1029/JC090iC03p05045.

[*Hunke et al.*(2011)*Hunke, Notz, Turner, and Vancoppenolle*] Hunke, E. C., D. Notz, A. K. Turner, and M. Vancoppenolle (2011), The multiphase physics of sea ice: a review for model developers, *The Cryosphere*, *5*(4), 9891009, doi:10.5194/tc-5-989-2011.

[*Huwald et al.*(2005a)*Huwald, Tremblay, and Blatter*] Huwald, H., L.-B. Tremblay, and H. Blatter (2005a), Reconciling different observational data sets from surface heat budget of the arctic ocean (SHEBA) for model validation purposes, *J. Geophys. Res.*, *110*(C5), C05,009, doi:10.1029/2003JC002221.

[*Huwald et al.*(2005b)*Huwald, Tremblay, and Blatter*] Huwald, H., L.-B. Tremblay, and H. Blatter (2005b), A multilayer sigma-coordinate thermodynamic sea ice model: Validation against surface heat budget of the arctic ocean (SHEBA)/Sea ice model intercomparison project part 2 (SIMIP2) data, *J. Geophys. Res.*, *110*(C5), C05,010, doi:10.1029/2004JC002328.

[*Jeffery et al.*(2011)*Jeffery, Hunke, and Elliott*] Jeffery, N., E. C. Hunke, and S. M. Elliott (2011), Modeling the transport of passive tracers in sea ice, *J. Geophys. Res.*, *116*(C7), C07,020, doi:10.1029/2010JC006527.

[*Jones et al.*(2012)*Jones, Ingham, and Eicken*] Jones, K. A., M. Ingham, and H. Eicken (2012), Modeling the anisotropic brine microstructure in first-year arctic sea ice, *J. Geophys. Res.*, *117*(C2), C02,005.

[*Kovacs*(1997)] Kovacs, A. (1997), Sea ice. part 1. bulk salinity versus ice floe thickness, *CRREL Report*, *96-7*, .

[*Lecomte et al.*(2011)*Lecomte, Fichefet, Vancoppenolle, and Nicolaus*] Lecomte, O., T. Fichefet, M. Vancoppenolle, and M. Nicolaus (2011), A new snow thermodynamic scheme for large-scale sea-ice models, *Ann. Glaciol.*, *52*(57), 337346.

[*Lei et al.*(2010)*Lei, Li, Cheng, Zhang, and Heil*] Lei, R., Z. Li, B. Cheng, Z. Zhang, and P. Heil (2010), Annual cycle of landfast sea ice in prydz bay, east antarctica, *J. Geophys. Res.*, *115*(C2), C02,006.

[*Levenberg*(1944)] Levenberg, K. (1944), A method for the solution of certain non-linear problems in least squares, *Quarterly Journal of Applied Mathmatics*, *II*(2), 164168.

[*Malmgren*(1927)] Malmgren, F. (1927), *On the properties of sea-ice: Norwegian North Polar Expedition with the MAUD, 1918-1925, Sci*, – pp., Results.

[*Massonnet et al.*(2011)*Massonnet, Fichefet, Goosse, Vancoppenolle, Mathiot, and Beatty*] Massonnet, F., T. Fichefet, H. Goosse, M. Vancoppenolle, P. Mathiot, and C. K. Beatty (2011), On the influence of model physics on simulations of arctic and antarctic sea ice, *Cryosphere*, *5*(3), 687699, doi:10.5194/tc-5-687-2011.

[*Maykut and Untersteiner*(1971)] Maykut, G. A., and N. Untersteiner (1971), Some results from a time-dependent thermodynamic model of sea ice, *J. Geophys. Res.*, *76*(6), 1550&, doi:10.1029/JC076i006p01550.

[*Nakawo and Sinha*(1981)] Nakawo, M., and N. K. Sinha (1981), Growth-rate and salinity profile of 1st-year sea ice in the high arctic, *J. Glaciol.*, *27*(96), 315330.

[*Notz*(2005)] Notz, D. (2005), Thermodynamic and fluid-dynamical processes in sea ice, Ph.D. thesis, Univ. of Cambridge,Cambridge, U.K.

[*Notz and Worster*(2006)] Notz, D., and M. G. Worster (2006), A one-dimensional enthalpy model of sea ice, *Ann. Glaciol.*, *44*(1), 123–128, doi:10.3189/172756406781811196.

[*Notz and Worster*(2008)] Notz, D., and M. G. Worster (2008), In situ measurements of the evolution of young sea ice, *J. Geophys. Res.*, *113*(C3), C03,001, doi:10.1029/2007JC004333.

[*Notz and Worster*(2009)] Notz, D., and M. G. Worster (2009), Desalination processes of sea ice revisited, *J. Geophys. Res.*, *114*(C5), C05,006, doi:10.1029/2008JC004885.

[*Oertling and Watts*(2004)] Oertling, A. B., and R. G. Watts (2004), Growth of and brine drainage from NaCl-H2O freezing: A simulation of young sea ice, *J. Geophys. Res.*, *109*(C4), C04,013, doi:10.1029/2001JC001109.

[*Perovich et al.*(2012)*Perovich, Richter-Menge, Elder, Arbetter, Claffey, and Polashenski*] Perovich, D., J. Richter-Menge, B. Elder, T. Arbetter, K. Claffey, and C. Polashenski (2012), Observing and understanding climate change: Monitoring the mass balance, motion, and thickness of arctic sea ice.

[*Perovich et al.*(1999)] Perovich, D. K., et al. (1999), Year on ice gives climate insights, *Eos Trans. AGU*, *80*(41), 481–486, doi:10.1029/EO080i041p00481-01.

[*Petrich et al.*(2004)*Petrich, Langhorne, and Sun*] Petrich, C., P. J. Langhorne, and Z. F. Sun (2004), Numerical simulation of sea ice growth and desalination, in *Proceedings of the 17th International Symposium on Ice*, vol. 3, pp. 68–78.

[*Petrich et al.*(2006)*Petrich, Langhorne, and Sun*] Petrich, C., P. J. Langhorne, and Z. F. Sun (2006), Modelling the interrelationships between permeability, effective porosity and total porosity in

sea ice, *Cold Regions Science and Technology*, *44*(2), 131144, doi: 10.1016/j.coldregions.2005.10.001.

[*Pringle et al.*(2009)*Pringle, Miner, Eicken, and Golden*] Pringle, D. J., J. E. Miner, H. Eicken, and K. M. Golden (2009), Pore space percolation in sea ice single crystals, *J. Geophys. Res.*, *114*(C12), C12,017, doi: 10.1029/2008JC005145.

[*Rees Jones and Worster*(2012a)] Rees Jones, D. J., and M. G. Worster (2012a), Fluxes through steady chimneys in a mushy layer during binary alloy solidification, *Submitted to J. Fluid Mech.*

[*Rees Jones and Worster*(2012b)] Rees Jones, D. J., and M. G. Worster (2012b), A simple dynamical model for gravity drainage of brine from growing sea ice, *submitted to Geophys Res Lett.*

[*Roscoe et al.*(2011)*Roscoe, Brooks, Jackson, Smith, Walker, Obbard, and Wolff*] Roscoe, H. K., B. Brooks, A. V. Jackson, M. H. Smith, S. J. Walker, R. W. Obbard, and E. W. Wolff (2011), Frost flowers in the laboratory: Growth, characteristics, aerosol, and the underlying sea ice, *J. Geophys. Res.*, *116*(D12), D12,301.

[*Saenz and Arrigo*(2012)] Saenz, B. T., and K. R. Arrigo (2012), Simulation of a sea ice ecosystem using a hybrid model for slush layer desalination, *J. Geophys. Res.*, *117*(C5), C05,007.

[*Schwerdtfeger*(1963)] Schwerdtfeger, P. (1963), The thermal properties of sea ice, *J. Glaciol*, *4*(36), 789807.

[*Semtner*(1976)] Semtner, A. J. (1976), Model for thermodynamic growth of sea ice in numerical investigations of climate, *J. Phys. Oceanogr.*, *6*(3), 379389.

[*Tait and Jaupart*(1992)] Tait, S., and C. Jaupart (1992), Compositional convection in a reactive crystalline mush and melt differentiation, *J. Geophys. Res.*, *97*(B5), 67356756.

[*Vancoppenolle et al.*(2010)*Vancoppenolle, Goosse, de Montety, Fichefet, Tremblay, and Tison*] Vancoppenolle, M., H. Goosse, A. de Montety, T. Fichefet, B. Tremblay, and J.-L. Tison (2010), Modeling brine and nutrient dynamics in antarctic sea ice: The case of dissolved silica, *J. Geophys. Res.*, *115*(C2), C02,005, doi:10.1029/2009JC005369.

[*Wells et al.*(2010)*Wells, Wettlaufer, and Orszag*] Wells, A. J., J. S. Wettlaufer, and S. A. Orszag (2010), Maximal potential energy transport: A variational principle for solidification problems, *Phys. Rev. Lett.*, *105*(25), 254,502, doi:10.1103/PhysRevLett.105.254502.

[*Wettlaufer et al.*(1997)*Wettlaufer, Worster, and Huppert*] Wettlaufer, J. S., M. G. Worster, and H. E. Huppert (1997), Natural convection during solidification of an alloy from above with application to the evolution of sea ice, *J. Fluid Mech.*, *344*, 291–316, doi:10.1017/S0022112097006022.

[*Widell et al.*(2006) *Widell, Fer, and Haugan*] Widell, K., I. Fer, and P. M. Haugan (2006), Salt release from warming sea ice RID g-2701-2010, *Geophys. Res. Lett.*, *33*(12), L12,501, doi:10.1029/2006GL026262.

[*Wilkins*(2010)] Wilkins, N. (2010), Thermodynamics of thin sea ice, Ph.D. thesis, Meteorological Institut, University of Hamburg, Germany.

[*Winton*(2000)] Winton, M. (2000), A reformulated three-layer sea ice model, *J. Atmos. Oceanic Technol.*, *17*(4), 525531.

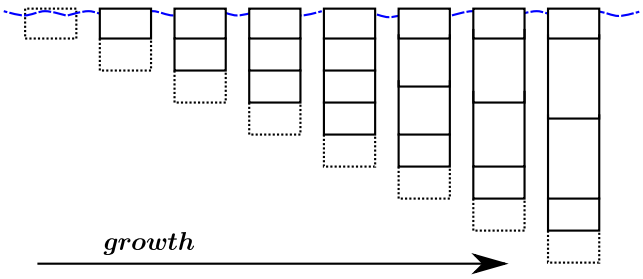

Figure 1: Semi-adaptive grid evolution during growth for N=5, N_{top}=1, N_{mid}=2, N_{bot}=2 (see subsection 2.2).

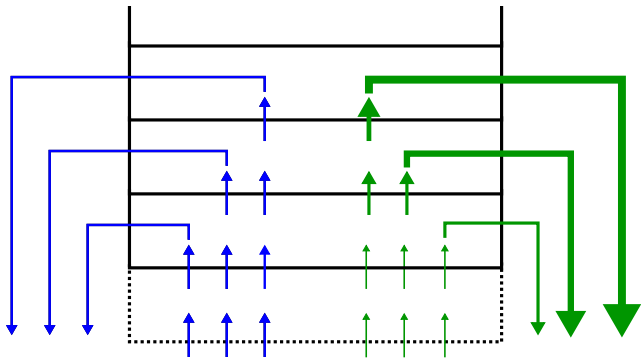

Figure 2: Brine fluxes (blue) and resulting salinity fluxes (green) of the convective gravity drainage parametrization in the bottom ice layers (see subsection 3.2). Arrow thickness indicates flux strength.

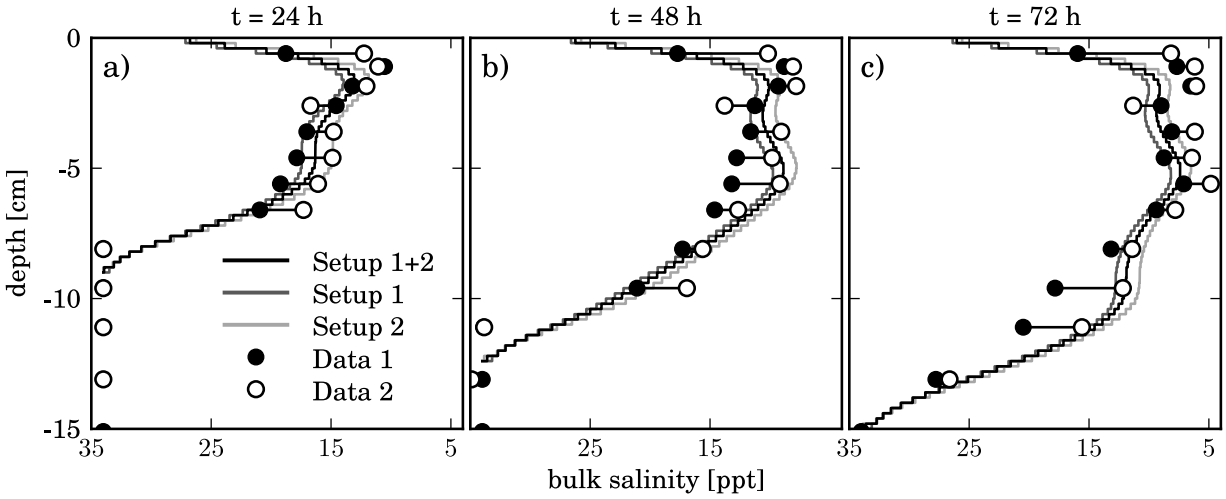

Figure 3: Bulk salinity measurements (dots) at different depths and corresponding model profiles at a) t=24h, b) t=48h, c) t=72h. The free parameters of the gravity drainage parametrization of Model 1 were optimized to fit Data 1, of Model 2 to fit Data 2, and of Model 1+2 to fit the average of Data 1 and Data 2. Grid parameters: N=90, $\triangle z_0$=0.2 cm See subsection 4.1 for details on experimental setup and instrumentation.

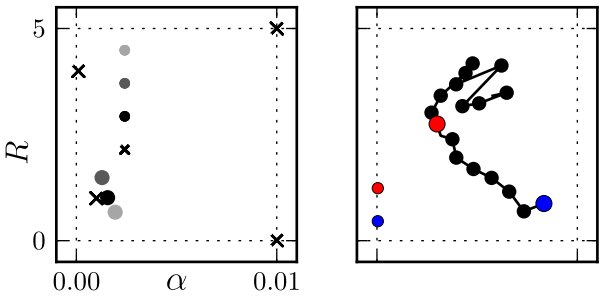

Figure 4: a) Values of R_{crit} and α derived by the Levenberg-Marquardt optimization algorithm for given sets of salinity measurements ('1+2' is the average of sets '1' and '2'). For all initial parameter values (marked by an x) the optimization results were identical. (b) Optimization results of R_{crit} and α for different vertical grid spacing dz. dz increases from 2 to 20 mm in 1 mm steps. Neighboring steps (i.e. 3 mm and 4 mm) are connected by a line. Note the different scales of subfigure a and b.

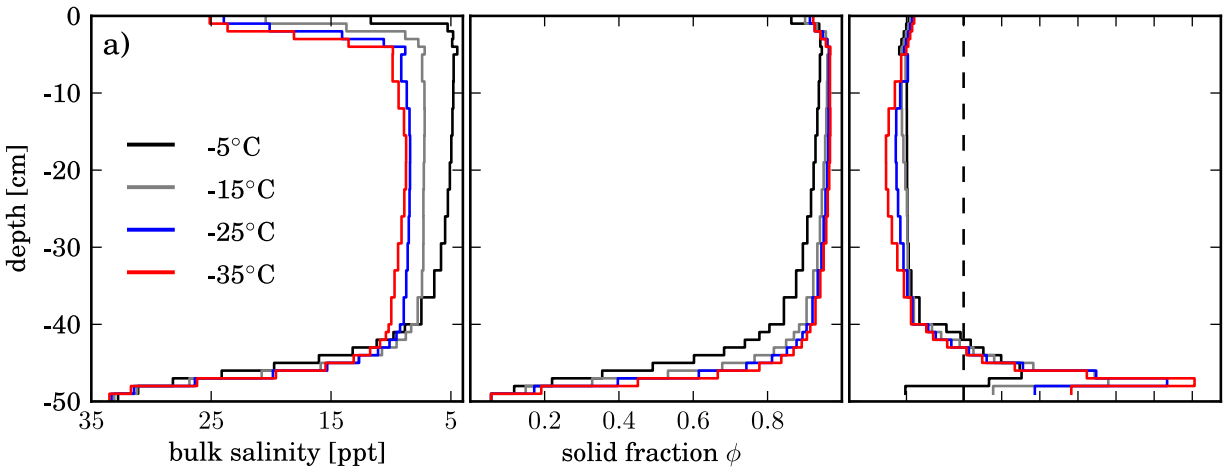

Figure 5: a) Bulk salinity, b) solid fraction, and c) Rayleigh number profiles of freezing NaCl from a fixed temperature. Simulations were run until the ice thickness reached 50 cm. Please notice that the scale of the x-axis in subfigure c) changes above 2. All layers with R greater than the critical Rayleigh number of 1.01 are convectively unstable. Grid parameters: N=25, N_{top}=5, N_{bot}=10, $\triangle z_0$=1cm

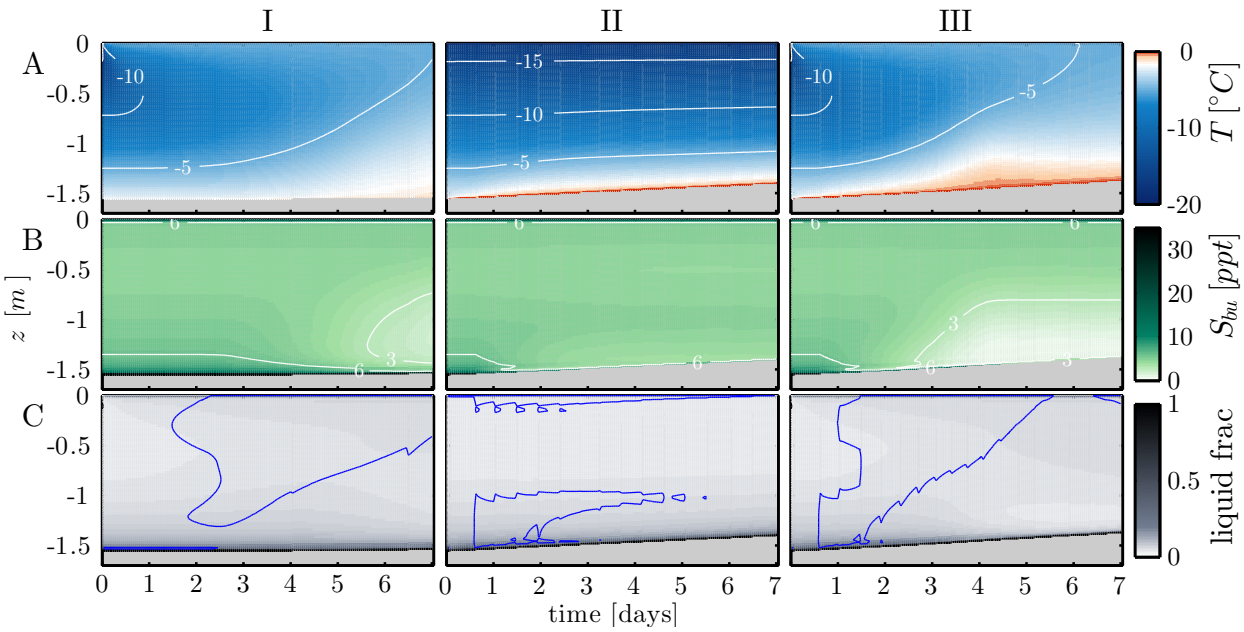

Figure 6: (A) temperature, (B) bulk salinity, and (C) liquid volume fraction over one week. The blue line in row C encloses convectively unstable layers. Beginning from identical stable initial conditions: experiment I raises the top temperature from -16.7° to -5° C, experiment II increases the oceanic heat flux from 20 to 100W, and experiment III combines experiment I and II. Grid parameters: N=70, N_{top}=5, N_{bot}=5, $\triangle z_0$=1cm

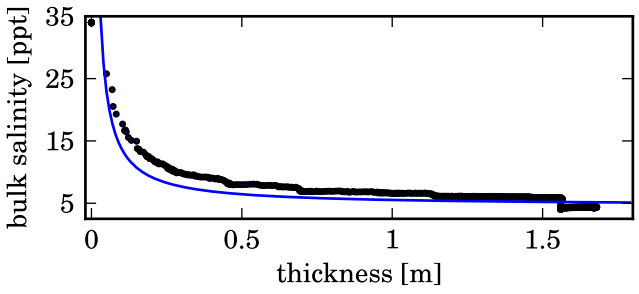

Figure 7: Reanalysis-forced daily model values of bulk salinity vs ice thickness (dots) and empirical relation of [*Kovacs*(1997),].

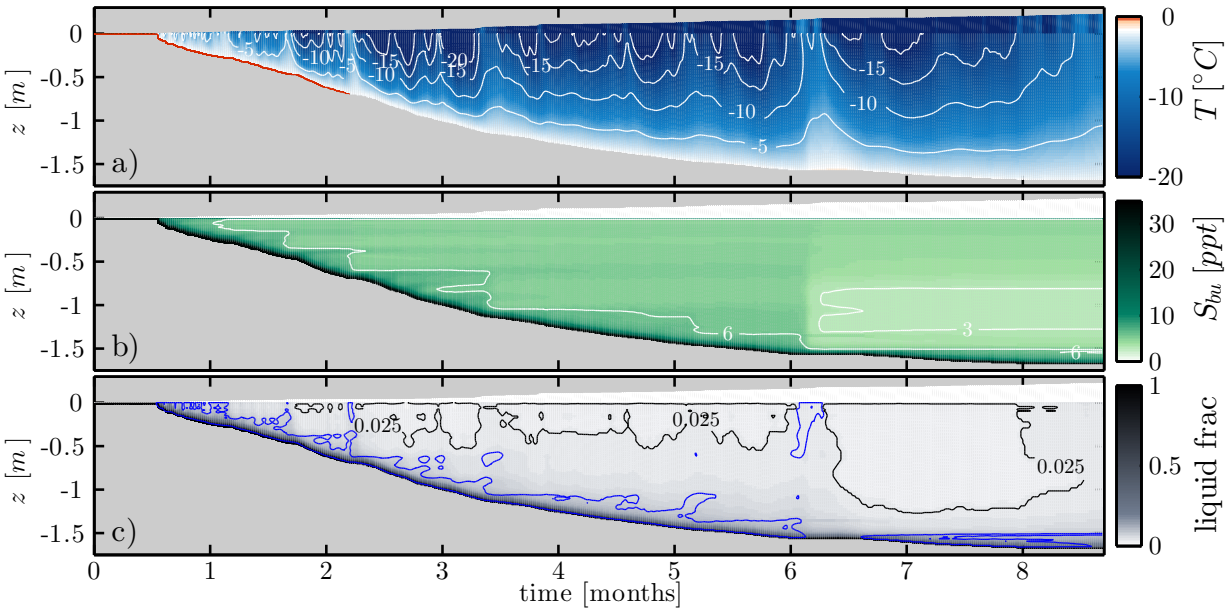

Figure 8: a) Temperature, b) bulk salinity, c) and liquid volume fraction over a growth season (see section 6). In subfigure c) the blue line encloses convectively unstable layers, and the black line encloses regions with a liquid fraction below 2.5 %. The single snow layer on top of the sea ice lies above $z = 0$. Grid parameters: N=70, N_{top}=10, N_{bot}=20, $\triangle z_0$=1cm

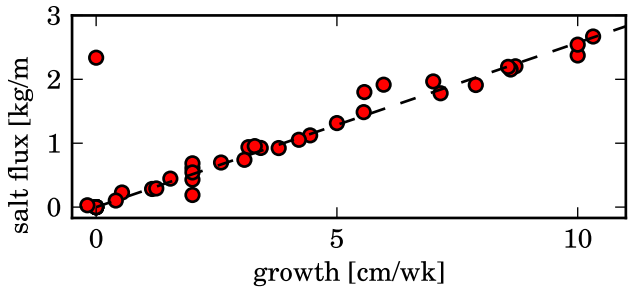

Figure 9: Reanalysis-forced weekly summed values of modeled salt flux vs growth speed.

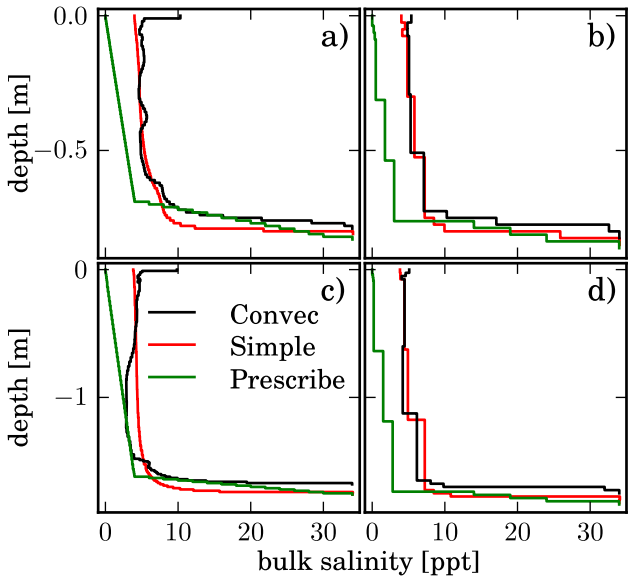

Figure 10: Case study salinity profiles of the convective and simple parametrization for two different vertical grids. a) Grid parameters: N=70, N_{top}=5, N_{bot}=5, $\triangle z_0$=1cm. b) Grid parameters: N=10, N_{top}=3, N_{bot}=4, $\triangle z_0$=5cm

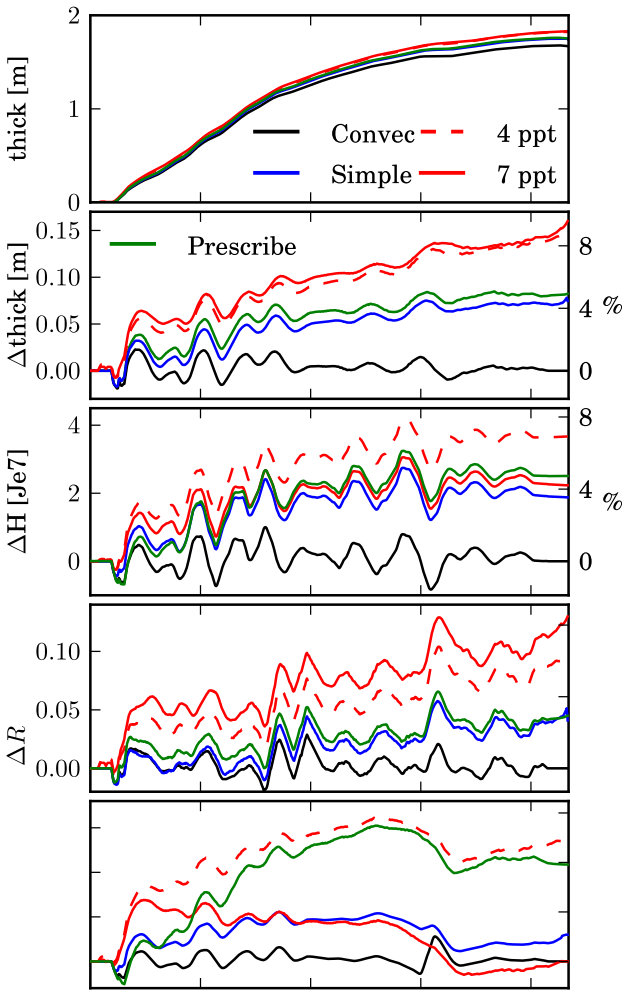

Figure 11: a) Thickness, and differences b) of thickness, c) of total enthalpy, d) of thermal resistance, and e) of fresh water column for the four salinity approaches. 'Convec': convective parametrization, 'Simple': simple parametrization, '4 ppt': initial salinity of 4 ppt, '7 ppt': initial salinity of 7 ppt. Differences are calculated by first subtracting a moving monthly average of the convective parametrization, and then applying a moving weekly average to reduce the noise. The percentages marked on the right y-axis of subfigures b) to e) are the left y-axis values divided by the end values of 'convec'.